Effect of powder purification by heat-treatment on the creep behaviour of dense boron carbide monoliths

L. Roumiguier, G. Antou, N. Pradeilles, A. Jankowiak, E. Zapata-Solvas, W.E. Lee, A. Maître

Effect of powder purification by heat-treatment on the creep behaviour of dense boron carbide monoliths

L. Roumiguier [a,b], G. Antou [b], N. Pradeilles [b], A. Jankowiak [a], E. Zapata-Solvas [c], W. E. Lee [c], A. Maître [b]

[a] DEN-Service de Recherches Métallurgiques Appliquées, CEA, Université Paris-Saclay, F-91191, Gif-sur-Yvette, France.
[b] Univ. Limoges, CNRS, IRCER, UMR 7315, F-87000 Limoges, France.
[c] Department of Materials, Imperial College London, London, UK.

Corresponding author
G. Antou : guy.antou@unilim.fr

Abstract:

High temperature compressive creep tests have been performed at 1650-1750 °C under applied stresses of 50-150 MPa on sintered boron carbide samples exhibiting high relative density and a mean grain size of 0.5 µm. The creep behaviour of two types of materials, sintered by spark plasma sintering from both raw and heat-treated powders, are characterized. For both materials, the identification of creep parameters (*i.e.* apparent activation energy and stress exponent values) coupled with TEM structural observations suggest a power law creep regime controlled by dislocation glide, which is limited by the presence of twins. However, the TP material exhibits lower stationary strain rates. This improved creep resistance seems to be directly correlated to the stoichiometry modification of the carbide induced by the powder pre-heat treatment, *i.e.* increase of structural carbon content and slight decrease of oxygen amount.

Key words (5):

Boron carbide; ceramics; creep; dislocations; chemical composition.

1. Introduction

Boron carbide ceramics are commonly used in advanced applications. In fact, the high melting point of this material, around 2500 °C, coupled with a good thermal conductivity and an abrasive resistance close to the diamond, around 0.4, makes this material suitable for high temperature environments [1]. Moreover, boron carbide is commonly used in nuclear power plants due to a good neutron absorption cross-section, from 3840 barns at 0,025 eV to a few barns for fast neutrons [2]. As well, boron carbides are of great interest for the ballistic industry as a result of high hardness, close to 30 GPa [3], and good impact resistance [4].

These excellent properties result from specific characteristics of the B-B and B-C chemical bonds. The rhombohedral crystalline structure of boron carbide has already been discussed in the literature

[1,5–7]. There is a general agreement regarding the existence of a solid solution with the stable phase with a homogeneous range extending from 8 to 20 at. % C [8–10]. Within this solid solution, the cell parameter of boron carbide admits a modification with the amount of carbon [6]. Since the atomic radius of carbon is lower than the atomic radius of boron, increasing the carbon content in the boron carbide phase leads to a decrease of the *a* and *c* cell parameters [6]. According to literature, the mechanical properties of full dense monoliths depend on variation of chemical composition, *i.e.* carbide stoichiometry and presence of secondary phases such as free carbon [11–13]. Niihara *et al.* [11] emphasized that, for a B/C ratio higher than 4, increasing B content in boron carbide plates obtained by chemical vapor deposition resulted in reduction of hardness and toughness, which was attributed to reduction of bond strength in the boron carbide structure. At the opposite, for carbon concentrations higher than 20 at.% (*i.e.* B/C < 4), they have highlighted that hardness and toughness also decreases due to the presence of free carbon as secondary phase located at grain boundaries. In addition, in previous works [12,13], we have shown that the presence of structural oxygen in boron carbide lattice, leading to a boron oxycarbide phase, induces a decrease in both hardness and elastic properties for oxygen content higher than 2 wt.%.

Some studies have highlighted the benefit effect of impurities removing from starting powder on elasticity and hardness of boron carbide monoliths sintered by Spark Plasma Sintering (SPS), displayed in **Table 1**. For boron carbide nanopowders, Moshtaghioun *et al*. [14] and Cho *et al*. [15] recommend to treat the starting powder by methanol washing, or with an intermediary step during the SPS cycle [16] in order to remove the oxide impurities at the nanoparticle surfaces. The enhanced sinterability of treated nanopowders with an intermediary step during SPS has been proved, as denser materials with finer microstructure have been obtained for similar SPS parameters [14]. Therefore, Moshtaghioun *et al*. [16] showed that the purification treatment of the nanopowder allows enhancing the hardness from 22.8 to 32.5 GPa due to a better densification of materials at the same sintering temperature. From a boron carbide submicrometric powder which has been previously heat-treated under a controlled atmosphere (mixture of argon and 2.9 % of dihydrogen), Belon *et al.* [17] observed an improved mechanical strength, with an increase of flexural strength by 19 % at room temperature, as seen in **Table 1**. Additionally, for sample sintered from heat-treated submicrometric powder (grade HD20 from H.C. Starck), Moshtaghioun *et al*. [18,19] obtained a slight increase in hardness and fracture toughness. It can be attributed to smaller grain sizes of material sintered from heat-treated powder.

Although numerous studies were carried out on boron carbide mechanical properties at room temperature [20–24,18,25,26], only few works [17,27–30] are related to the characterization of the high temperature mechanical behaviour of boron carbide materials, *i.e.* within the range 1400-2000 °C. Moshtaghioun *et al.* [29] characterized the compressive creep behaviour of boron carbide ceramics sintered by SPS. These materials, with a mean grain size of 17 µm, were tested at 1600-1800 °C under 250-500 MPa under argon gaz atmosphere. The oxygen partial pressure was estimated to be less than 10^{-5} atm. Creep parameters, *i.e.* apparent activation energy and stress exponent values, were evaluated at approximately 632 kJ.mol^{-1} and 3 respectively. They also studied

the creep behaviour of finer boron carbides, with average grain sizes of 700 nm and 130 nm [30]. Based on an analytical model validated by experimental results, they suggested that the combination of increasing twin barriers and dislocations in mutual interaction is the rate-controlling mechanism of plasticity at high temperature.

The present work aims at investigating the effect of powder purification by heat-treatment on the creep behavior of dense boron carbide monoliths. To this purpose, two types of monoliths were sintered using the SPS method, the first one from as-received powder and the second one from purified powder by previous heat-treatment under controlled atmosphere. These monoliths exhibit a low residual porosity level and a fine microstructure (*i.e.* submicrometric mean grain size). Their creep resistance and the involved deformation mechanisms are then compared and correlated to their chemical composition, especially (oxy-)carbide stoichiometry (*i.e.* B/C and O/C ratios).

2. Experimental procedures

The starting material is a commercially available submicrometric boron carbide powder (Grade HD20, H.C. Starck, Germany). As previously noticed in the literature [17], this commercial boron carbide powder of high purity contains some secondary phases, *i.e.* graphite and boric acid. To decrease the impurity content, a batch of powder have been heat treated at 1350 °C during 5h under a controlled atmosphere (mixture of argon and 2.9 % of dihydrogen), as recommended by Belon *et al.* [17]. X-ray diffraction (XRD) analyses were conducted on both powders using a Bruker D8 Advance device (Germany; LYNXEYE XE-T detector, Cu-Kα radiation, Ni filter). The XRD pattern acquisition conditions are: angular step of 0.02°, time per step of 0.3 s, angle range 10–120°. As carried out in our previous work [12,13], free carbon amounts were determined according to the method depicted by Beauvy *et al*. [31], using relative intensities of XRD diffraction lines of powders with various quantities of added graphite. The contents in oxygen, hydrogen and total carbon of powders (raw powder and treated powder, RP and TP, respectively) were measured by elemental chemical analyses (EMIA-321V for carbon, and EMGA-830 for oxygen and hydrogen from HORIBA, Ltd., Japan).

The raw and the heat-treated powders have been sintered by SPS using a Dr. Sinter 825 SPS device (Fuji Electronics Industrial Co. Ltd., Japan). Powder compacts were sintered under vacuum at 1650 °C for 5 min under 75 MPa. The sintering temperature was reached using a heating rate of 200 °C.min^{-1}. Sintered samples exhibit a relative density higher than 98 %, therefore identified thermomechanical properties are not altered by porosity.

Samples were machined to dimensions of 3 mm x 3 mm x 5 mm and polished on their square parallel surfaces. Compressive creep tests were carried out using a custom-built testing rig consisting of an MRF Vacuum furnace (Materials Research Furnaces, LLC, USA) mounted in a 100 kN universal test frame using a 25 kN load cell. Samples were protected from direct contact with the graphite punches during the test by SiC rods. The test temperature was reached at 15 °C.min^{-1} and all

creep tests were performed under vacuum. The load was applied in 5 min once the test temperature was reached, to carry out deformation under thermal equilibrium conditions, and the strain was recorded versus time. For both monoliths, creep tests have been carried out by varying one experimental parameter at the time, *i.e.* in isobar or isothermal conditions with temperatures of 1650, 1700, 1750 °C under 100 MPa and then with applied stresses of 50, 100, 150 MPa at 1750 °C.

Thin slices of materials before and after creep tests were produced using a focused ion beam electron microscope (FEI Strata DB 235 instrument, FEI Company, now Thermo Fisher Scientific, Waltham, MA). The microstructures of sintered samples were observed on a FEI Tecnai G2-20 twin transmission electron microscope, equipped with an energy dispersive spectrometer (EDS) to analyze local chemical composition. Mean grain sizes were determined measuring at least 120 grains on TEM micrographs. XRD measurements were also conducted, and the chemical composition of RP and TP monoliths were determined using same methods than the ones used for powders.

3. Results and discussion

3. 1. Characterization of starting powders

As shown in **Figure 1**, the starting powder consists of submicronic particles with angular shapes. Sizes of the particles are mainly ranged from 60 to 700 nm. Boron carbide and free carbon crystallized under the graphite form are identified within both RP and TP powders by XRD (**Figure 2**). Moreover, as reported in **Table 2**, content of free carbon slightly decreases from 0.57 to 0.41 wt.% during the heat treatment. Indeed, as mentioned by Belon *et al.* [17], carbon is likely to react during the heat treatment with hydrogen to form hydrocarbons. In addition, contrary to TP power, boric acid is detected in RP powder by XRD (**Figure 2**). This is confirmed by chemical analyzes (**Table 2**), where oxygen and especially hydrogen contents are lower for TP powder. In fact, boric acid is expected to be removed during the heat treatment, following the reactions [32,33]:

$$H_3BO_3 = HBO_2 + H_2O \quad (1)$$

$$HBO_2 + HBO_2 = (HBO_2 \cdot HBO_2)\ \text{complex} \quad (2)$$

$$(HBO_2 \cdot HBO_2) = B_2O_3 + H_2O \quad (3)$$

$$B_2O_3\ (s,l) = B_2O_3\ (g) \quad (4)$$

The volatilization of boron oxide begins at 900 °C under atmospheric pressure [32], which is under the temperature applied during the heat-treatment of raw powder.

3. 2. Structural and chemical characterizations of sintered samples

As shown by XRD analyzes (**Figure 2**), boric acid is no longer detected after sintering in RP monolith. Indeed, chemical analyzes only reveal traces of hydrogen within dense samples (**Table 2**). Boric acid would have volatilized following the previous reactions during the SPS treatment. The remaining oxygen is therefore considered to be structural, leading to a boron oxycarbide. The

calculated stoichiometries of boron oxycarbides are very close and are $B_{3.87}CO_{0.04}$ and $B_{3.75}CO_{0.03}$ for RP and TP monoliths, respectively.

Figure 3a and **3b** depicts micro-structural observations conducted by TEM for sintered samples from raw (RP) and heat-treated (TP) powders. Their median grain sizes are 550 ± 50 nm and 510 ± 50 nm respectively. In addition, RP material contained few quantities of partially crystalized intergranular phases. Their analyzes by Energy-Dispersive X-Ray Spectroscopy (EDX) and SAED pattern reveal crystallized carbon under graphite form (**Figure 4**), showing sometimes an "onion-like" structure with rolled-up turbostratic carbon layers [34–36]. Moreover, some amorphous phases surrounding pores can be observed in RP samples, mainly composed of oxygen and silicon. However, they are no longer observed in TP material. This difference can be explained by the powder heat-treatment, in which those oxygen-rich phases have volatilized.

3. 3. Creep behaviour of sintered samples

The creep behavior of both sintered boron carbide monoliths are compared in order to analyze the effect of the powder purification and to establish correlations with modification of the chemical composition.

Figure 5.a and **5b** display the typical evolutions of strain and strain rate measured during creep tests for both monoliths. For these applied creep conditions (*i.e.* at 1750 °C under 100 MPa), the RP and TP samples reach the stationary creep stage in about 1800 seconds and exhibit stationary strain rates of $1.79.10^{-5}$ and $3.80.10^{-6}$ s^{-1}, respectively. In fact, as shown in **Table 3**, for all the applied creep conditions, the TP monolith reveals higher creep resistance, *i.e.* lower stationary strain rates on average by a factor of 6 compared to the ones of the RP material. Moreover, the values of different strain rates reported in literature for boron carbide ceramics are displayed in **Figure 6**. Abzianidze *et al.* [27] have measured higher stationary strain rates compared to our study, as expected concerning porous ceramics. Besides, Moshtaghioun *et al.* [29] have characterized micrometric boron carbides at the same temperature than for RP and TP materials, *i.e.* 1650 °C. They measured similar strain rates for higher stresses due to larger grain sizes. as usually observed in the literature [37]. Furthermore, Moshtaghioun *et al.* [30] also studied boron carbides exhibiting finer microstructures. Similar stationary strain rates were determined between nanometer-scaled ceramics and our submicronic materials, even if these nanometer-scaled ceramics were crept at lower temperatures (< 150 °C). This observation might constitute a disadvantage concerning the utilization of nanometric boron carbides under high strain and temperature.

In order to study the dependence of the creep behaviour to applied stress and temperature for each material, the creep data have been analyzed using this following conventional creep equation [38]:

$$\dot{\varepsilon} = A\frac{\sigma^n}{k_B T}\exp\left(-\frac{Q}{RT}\right) \qquad (5)$$

with $\dot{\varepsilon}$ the stationary strain rate, σ the applied stress, T the temperature, n the stress exponent, Q the apparent activation energy, R the ideal gas constant, k_B the Boltzmann constant and A a stress and

temperature independent constant reflecting the dependence of the strain rate to the microstructural features of the material (grain size, composition).

As noticeable in **Figure 3c** and **3d**, no significant evolution of grain size has been observed for both materials after creep experiments in the most severe thermomechanical conditions (*i.e.* at a soaking temperature of 1750 °C under an applied stress of 150 MPa). Therefore, the conducted creep experiments allow distinguish the effects of stress and temperature without microstructural effect, such as grain growth.

The identification of the apparent activation energy (Q) has been carried out in isobar conditions (*i.e.* applied stress of 100 MPa) by varying the temperature between 1650 and 1750 °C. **Figure 7a** represents the strain rate as a function of temperature. From this Arrhenius plotting, Q value can be determined from the slope. The calculated apparent activation energies are 974 ± 120 kJ.mol^{-1} and 1 076 ± 101 kJ.mol^{-1} for the RP and TP monoliths, respectively. Similarly, n was deduced with a constant test temperature of 1750 °C and by changing the stress within the range 50 - 150 MPa, as plotted in **Figure 7b**. Stress exponent values are then equal to 4.2 ± 0.4 and 4.8 ± 0.2, for the RP and TP materials, respectively. Both materials exhibit similar creep parameters, namely apparent activation energy and stress exponent values. The analogous dependence of strain rates to applied stress and temperature suggests an identical viscoplastic deformation mechanism. A stress exponent value around 4.5 reveals a power law creep regime usually attributed to the dislocation glide and climb, controlled by climb [37]. However, Moshtaghioun *et al.* [30], thanks to the development of an analytical model validated by experimental results, have shown that fine-grained boron carbides do not follow the classical power-law for high-temperature creep in ceramics. This breakdown of the classical power law creep is effective for boron carbides with grain size below a critical value estimated to be around 1 µm. Indeed, twinned grains (see contrasted straight stripes indicated by white arrows in **Figure 3**) are commonly observed in boron carbide due to its relatively low stacking fault energy (76 mJ/m² [39]). These twins act as strong barriers for dislocation glide and decrease the effective grain size. Moshtaghioun *et al.* hence suggested that the plastic flow within fine-grained boron carbide is controlled by a mutual interaction between the increase of twin barriers and dislocations motion. Dislocations can over-pass them by a mechanically and thermally activated process [30]. When the coupling between dislocations and twins becomes strong, *i.e.* for fine-grained boron carbides, a power-law creep is not acceptable as a constitutive equation for high-temperature deformation. Therefore, Moshtaghioun *et al.* [30] suggested an analytical model based on the classical Orowan relation, which relates strain rate to the dislocation density and their velocity, associated with the hardening of material, inducing an internal stress field within the polycrystalline material. In this term, the interaction between dislocations and twins was introduced by limiting the mean free path of dislocations by the distance between two consecutive twin planes [30]. In this case, the creep parameters are no longer constants for given stress and temperature, and are called "effective creep parameters".

In the present work, TEM structural observations of crept samples at a moderate total strain around 10 % (**Figure 3c** and **d**) has confirmed the presence of twins (white arrows) and dislocations

(black arrows) within boron carbide grains. In addition, the creep parameters identified here fit well with the values predicted by the analytical model of Moshtaghioun *et al.* [30], as represented in **Figure 8.** The effective apparent activation energy predicted by this model considers an intrinsic activation energy for self-diffusion of 385 kJ.mol^{-1}, which corresponds to the reported value for volume diffusion of carbon in boron carbide [40]. Consequently, based on the identified effective creep parameters in accordance with the model of Moshtaghioun *et al.*, it appears that the creep behaviour of both monoliths studied here involves similar deformation mechanisms, namely a dislocation-driven plasticity mechanism that is rate-controlled by lattice diffusion of C.

The improvement of the creep resistance induced by the pre-heat treatment of the powder is correlated to a modification of the chemical composition of the boron oxycarbides. In fact, this pre-heat treatment has mainly altered the oxycarbide stoichiometry, as the chemical formula of RP material is $B_{3.87}CO_{0.04}$ whereas TP is $B_{3.75}CO_{0.03}$. Therefore, the oxycarbide of the TP material exhibits an increase of structural carbon content and slight decrease of oxygen amount. This modification of the stoichiometry may affect the number of vacancies on the carbon or boron sub-lattice.

4. Conclusion

High temperature creep tests were performed on spark plasma sintered boron carbide samples, exhibiting high relative density and a mean grain size of 0.5 µm. Two types of materials were studied from both raw and heat-treated powders to study the effect of the chemical composition, in particular carbide stoichiometry, on the creep behaviour. The effective apparent activation energies Q determined from creep data were 974 ± 120 kJ/mol for RP and 1 076 ± 101 kJ/mol for TP. The measured stress exponent values were respectively 4.2 ± 0.4 and 4.8 ± 0.2, revealing a power law creep regime controlled by glide of dislocations in mutual interaction with increasing twin barriers. The material from heat-treated powder exhibits an improved creep resistance due to an increase of structural oxygen content. In the light of these results, the heat-treatment of boron oxycarbide powders have a significant effect on creep behaviour of sintered materials. This additional step is therefore recommended for boron carbides used in severe conditions of pressure and temperature.

Acknowledgements

The authors are grateful to the JECS Trust for funding the mobility to the Imperial College of London to realize creep tests (Contract No. 2017297). The authors would like to acknowledge F. Réjasse and R. Belon from IRCER institute, Daniel Glymond from the Imperial College of London and Ahmed Addad from University of Lille, respectively for their help in the achievement of this work.

Bibliography

[1] F. Thevenot, Boron carbide - a comprehensive review, J. Eur. Ceram. Soc. 6 (1990) 205–225. https://doi.org/10.1016/0955-2219(90)90048-K.

[2] D. Simeone, Contribution à l'étude de l'évolution du carbure de bore sous irradiation neutronique, Thèse du CEA Saclay, ISSN 0429-3460, Rapport CEA-R-5858, 1999.

[3] A.K. Suri, C. Subramanian, J.K. Sonber, T.S.R.C. Murthy, Synthesis and consolidation of boron carbide: a review, Int. Mater. Rev. 55 (2010) 4–40. https://doi.org/10.1179/095066009X12506721665211.

[4] V. Domnich, S. Reynaud, R.A. Haber, M. Chhowalla, Boron carbide: structure, properties and stability under stress, J. Am. Ceram. Soc. 94 (2011) 3605–3628. https://doi.org/10.1111/j.1551-2916.2011.04865.x.

[5] H.L. Yakel, Recent developments in the structural crystallography of boron and the higher borides, AIP Conf. Proc. 140 (1986) 97–108.

[6] T.L. Aselage, R.G. Tissot, Lattice constants of boron carbides, J. Am. Ceram. Soc. 75 (1992) 2207–2212.

[7] K. Shirai, Electronic structures and mechanical properties of boron and boron-rich crystals (Part 2), J. Superhard Mater. 32 (2010) 336–345.

[8] M. Bouchacourt, F. Thevenot, The melting of boron carbide and the homogeneity range of the boron carbide phase, J. Common Met. 67 (1979) 327–331.

[9] M. Bouchacourt, F. Thevenot, Analytical investigations in the B-C system, J. Common Met. 82 (1981) 219–226.

[10] D. Gosset, M. Colin, Boron carbides of various compositions: An improved method for X-rays characterisation, J. Nucl. Mater. 183 (1991) 161–173.

[11] K. Niihara, A. Nakahira, T. Hirai, The effect of stoichiometry on mechanical properties of boron carbide, J. Am. Ceram. Soc. 67 (2006) C-13-C–14. https://doi.org/10.1111/j.1151-2916.1984.tb19158.x.

[12] F. Réjasse, M. Georges, N. Pradeilles, G. Antou, A. Maître, Influence of chemical composition on mechanical properties of spark plasma sintered boron carbide monoliths, J. Am. Ceram. Soc. 101 (2018) 3767–3772. https://doi.org/10.1111/jace.15707.

[13] L. Roumiguier, A. Jankowiak, N. Pradeilles, G. Antou, A. Maître, Mechanical properties of submicronic and nanometric boron carbides obtained by Spark Plasma Sintering: Influence of B/C ratio and oxygen content, Ceram. Int. 8 (2019) 9912–9918. https://doi.org/10.1016/j.ceramint.2019.02.033.

[14] B.M. Moshtaghioun, D. Gómez-García, A. Domínguez-Rodríguez, A.L. Ortiz, Enhancing the spark-plasma sinterability of B_4C nanopowders via room-temperature methylation induced purification, J. Eur. Ceram. Soc. 36 (2016) 2843–2848. https://doi.org/10.1016/j.jeurceramsoc.2016.04.008.

[15] N. Cho, K.G. Silver, Y. Berta, R.F. Speyer, N. Vanier, C.-H. Hung, Densification of carbon-rich boron carbide nanopowder compacts, J. Mater. Res. 22 (2007) 1354–1359. https://doi.org/10.1557/jmr.2007.0155.

[16] B.M. Moshtaghioun, A.L. Ortiz, D. Gómez-García, A. Domínguez-Rodríguez, Densification of B_4C nanopowder with nanograin retention by spark-plasma sintering, J. Eur. Ceram. Soc. 35 (2015) 1991–1998. https://doi.org/10.1016/j.jeurceramsoc.2014.12.021.

[17] R. Belon, G. Antou, N. Pradeilles, A. Maître, D. Gosset, Mechanical behaviour at high temperature of spark plasma sintered boron carbide ceramics, Ceram. Int. 43 (2017) 6631–6635. https://doi.org/10.1016/j.ceramint.2017.02.053.

[18] B.M. Moshtaghioun, F.L. Cumbrera, A.L. Ortiz, M. Castillo-Rodríguez, D. Gómez-García, Additive-free superhard B_4C with ultrafine-grained dense microstructures, J. Eur. Ceram. Soc. 34 (2014) 841–848. https://doi.org/10.1016/j.jeurceramsoc.2013.10.006.

[19] B.M. Moshtaghioun, D. Gomez-Garcia, A. Dominguez-Rodriguez, Richard.I. Todd, Grain size dependence of hardness and fracture toughness in pure near fully-dense boron carbide ceramics, J. Eur. Ceram. Soc. 36 (2016) 1829–1834. https://doi.org/10.1016/j.jeurceramsoc.2016.01.017.

[20] S. Hayun, V. Paris, M.P. Dariel, N. Frage, E. Zaretzky, Static and dynamic mechanical properties of boron carbide processed by spark plasma sintering, J. Eur. Ceram. Soc. 29 (2009) 3395–3400. https://doi.org/10.1016/j.jeurceramsoc.2009.07.007.

[21] P. Badica, S. Grasso, H. Borodianska, S.S. Xie, P. Li, P. Tatarko, M.J. Reece, Y. Sakka, O. Vasylkiv, Tough and dense boron carbide obtained by high-pressure (300 MPa) and low-temperature (1600°C) spark plasma sintering, J. Ceram. Soc. Jpn. 122 (2014) 271–275. https://doi.org/10.2109/jcersj2.122.271.

[22] M. Cengiz, B. Yavas, Y. Celik, G. Goller, O. Yucel, F.C. Sahin, Spark plasma sintering of boron carbide ceramics using different sample geometries and dimensions, Acta Phys. Pol. A. 125 (2014) 260–262. https://doi.org/10.12693/APhysPolA.125.260.

[23] X. Li, D. Jiang, J. Zhang, Q. Lin, Z. Chen, Z. Huang, Densification behavior and related phenomena of spark plasma sintered boron carbide, Ceram. Int. 40 (2014) 4359–4366. https://doi.org/10.1016/j.ceramint.2013.08.106.

[24] B.M. Moshtaghioun, A.L. Ortiz, D. Gómez-García, A. Domínguez-Rodríguez, Toughening of super-hard ultra-fine grained B_4C densified by spark-plasma sintering via SiC addition, J. Eur. Ceram. Soc. 33 (2013) 1395–1401.

[25] K. Sairam, J.K. Sonber, T.S.R.Ch. Murthy, C. Subramanian, R.K. Fotedar, P. Nanekar, R.C. Hubli, Influence of spark plasma sintering parameters on densification and mechanical properties of boron carbide, Int. J. Refract. Met. Hard Mater. 42 (2014) 185–192. https://doi.org/10.1016/j.ijrmhm.2013.09.004.

[26] M. Asadikiya, C. Zhang, C. Rudolf, B. Boesl, A. Agarwal, Y. Zhong, The effect of sintering parameters on spark plasma sintering of B_4C, Ceram. Int. 43 (2017) 11182–11188. https://doi.org/10.1016/j.ceramint.2017.05.167.

[27] T.G. Abzianidze, A.M. Eristavi, S.O. Shalamberidze, Strength and Creep in Boron Carbide (B_4C) and Aluminum Dodecaboride (α-AlB_{12}), J. Solid State Chem. 154 (2000) 191–193. https://doi.org/10.1006/jssc.2000.8834.

[28] G. De With, High temperature fracture of boron carbide: experiments and simple theoretical models, J. Mater. Sci. 19 (1984) 457–466. https://doi.org/10.1007/BF02403232.

[29] B.M. Moshtaghioun, D.G. García, A.D. Rodríguez, N.P. Padture, High-temperature creep deformation of coarse-grained boron carbide ceramics, J. Eur. Ceram. Soc. 35 (2015) 1423–1429. https://doi.org/10.1016/j.jeurceramsoc.2014.11.001.

[30] B.M. Moshtaghioun, D.G. García, A.D. Rodríguez, High-temperature deformation of fully-dense fine-grained boron carbide ceramics: Experimental facts and modeling, Mater. Des. 88 (2015) 287–293. https://doi.org/10.1016/j.matdes.2015.08.134.

[31] M. Beauvy, R. Angers, Method for the determination of free graphite in boron carbide, J - Common Met. 80 (1981) 227–233. https://doi.org/10.1016/0022-5088(81)90096-5.

[32] J.P. Viricelle, P. Goursat, D. Bahloul-Hourlier, Oxidation behaviour of a boron carbide based material in dry and wet oxygen, J. Therm. Anal. Calorim. 63 (2000) 507–515.

[33] V.G. Slutskii, E.S. Severin, L.A. Polenov, An Ab initio study of reactions in the H3BO3/B2O3/H2O system, Russ. J. Phys. Chem. B. 1 (2007) 549–552. https://doi.org/10.1134/S1990793107060061.

[34] D. Ugarte, Curling and closure of graphitic networks under electron-beam irradiation, Nature. 359 (1992) 707. https://doi.org/10.1038/359707a0.

[35] S. Iijima, Direct observation of the tetrahedral bonding in graphitized carbon black by high resolution electron microscopy, J. Cryst. Growth. 50 (1980) 675–683. https://doi.org/10.1016/0022-0248(80)90013-5.

[36] P.R. Marcoux, Réactivité et manipulation de nanotubes de carbone monocouches : fonctionnalisation de surface par greffage covalent et mise en oeuvre comme agent structurant., Thèse de l'Université d'Angers, 2002.

[37] W.R. Cannon, T.G. Langdon, Creep of ceramics - Part1: Mechanical characteristics, 18 (1983) 1–50.

[38] A.K. Mukherjee, J.E. Bird, J.E. Dorn, Experimental correlations for high-temperature creep, Trans. Am. Soc. Metals 62 (1969) 155-179.

[39] J. Freidel, Dislocations in Crystals, Oxford, New York, Pergamon Press, 1964.

[40] W. Borchert, A.R. Kerler, Kinetic analysis of boron carbide sintering, Metall. 29 (1975) 993–1002.

Tables

Table 1: *Literature features about effects of purification of starting power on boron carbide ceramics sintered by SPS.*

Starting powder	**Purification of powder**	**SPS conditions**			**Relative density** (%)	**Grain size** (nm)	**Vickers hardness** (GPa)	**Fracture toughness** ($MPa.m^{1/2}$)	**Flexural strength** (MPa)	**References**
		Pressure	**Max. Temperature**	**Dwell time**						
Tekna Plasma System	None	75 MPa	1600 °C	3 min	94.6	100	22.8 ±3	4.61 ± 0.3	-	[16]
Tekna Plasma System	1150 °C, 8h Ar(g)	75 MPa	1600 °C	3 min	97.5	180	32.5 ± 3	4.12 ± 0.3	-	[16]
Tekna Plasma System	Room temperature methylation	75 MPa	1600 °C	3 min	98	2900	31.7 ± 2.0	2.9 ± 0.2	-	[14]
HD20 H. C. Starck	None	75 MPa	1700 °C	3 min	100	690	36 ± 2	2.0 ± 0.1	-	[19]
HD20 H. C. Starck	High-energy ball-milling then 1350 °C, 8h, Ar(g)	75 MPa	1700 °C	3 min	98.8	450	37.0	2.9	-	[18]
HD20 H. C. Starck	None	75 MPa	1650 °C	5 min	> 98	600	42.6 ± 3.9	2.6 ± 0.2	320 ± 20	[17]
HD20 H. C. Starck	1350 °C, 5h Ar(g) + H_2(g)	75 MPa	1650 °C	5 min	> 98	500	39.6 ± 3.1	2.3 ± 0.2	400 ± 20	[17]

***Table 2**: Chemical composition of powders and sintered samples.*

Element		wt% O	wt% H	wt% C	wt% free C
Powder	RP	2.75 ± 0.07	0.19 ± 0.01	22.3 ± 0.4	0.57 ± 0.10
	TP	1.30 ± 0.01	0.08 ± 0.01	21.0 ± 0.2	0.41 ± 0.06
Bulk	RP	1.04 ± 0.01	0.01 ± 0.01	22.5 ± 0.2	-
	TP	0.82 ± 0.01	0.01 ± 0.01	23.0 ± 0.2	-

***Table 3:** Measured stationary strain rates for both monoliths.*

Starting powder	Soaking temperature T (°C)	Applied pressure σ (MPa)	Strain rate $\dot{\varepsilon}$ (s^{-1}) x 10^{-6}
RP Raw powder	1650	100	0.83 ± 0.08
	1700	100	5.15 ± 0.28
	1750	50	0.63 ± 0.05
	1750	100	17.86 ± 2.05
	1750	150	64.46 ± 2.68
TP Heat-treated powder	1650	100	0.16 ± 0.01
	1700	100	0.56 ± 0.05
	1750	50	0.13 ± 0.04
	1750	100	3.80 ± 0.20
	1750	150	21.71 ± 0.97

Figures captions

Figure 1: TEM micrograph of starting powder.
Figure 2: XRD patterns of raw powder (RP), heat-treated powder (TP) and related sintered samples.
Figure 3: TEM micrographs of sintered samples from (a, c) RP and (b, d) TP powders, (a, b) before and (c, d) after creep experiments at 1750 °C and 150 MPa. White arrows points out twins, black arrows points out dislocations and dotted-blue arrows points out amorphous phases.
Figure 4: TEM micrograph of (a) crystallized carbon impurity and (b) zoom at high resolution.
Figure 5: Evolution of strain versus time for (a) RP and (b) TP ceramics.
Figure 6: Comparison with the different strain rates determined for boron carbide ceramics in the literature.
Figure 7: Evolution of a) strain rate versus temperature under 100 MPa and b) strain rate versus applied stress at 1750 °C.
Figure 8: Evolutions of effective stress exponent (a) and activation energy (b) as a function of grain size from Moshtaghioun et al. [30] in black ; with our experimental points in color.

1-column fitting image: Figure 1, Figure 2, Figure 5, Figure 7, Figure 8

1.5-column fitting image: Figure 3, Figure 4

2-column fitting image: Figure 6

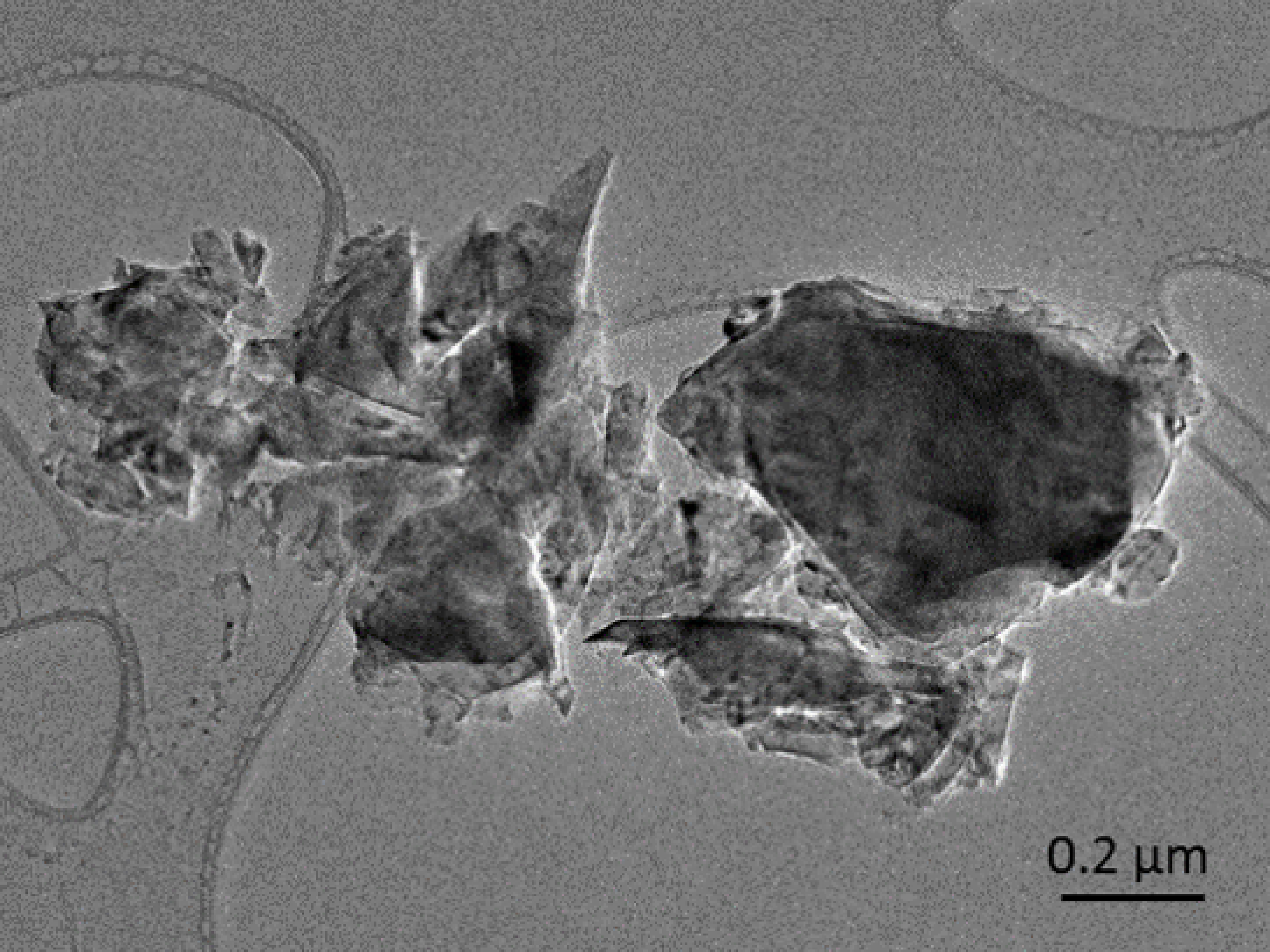
0.2 µm

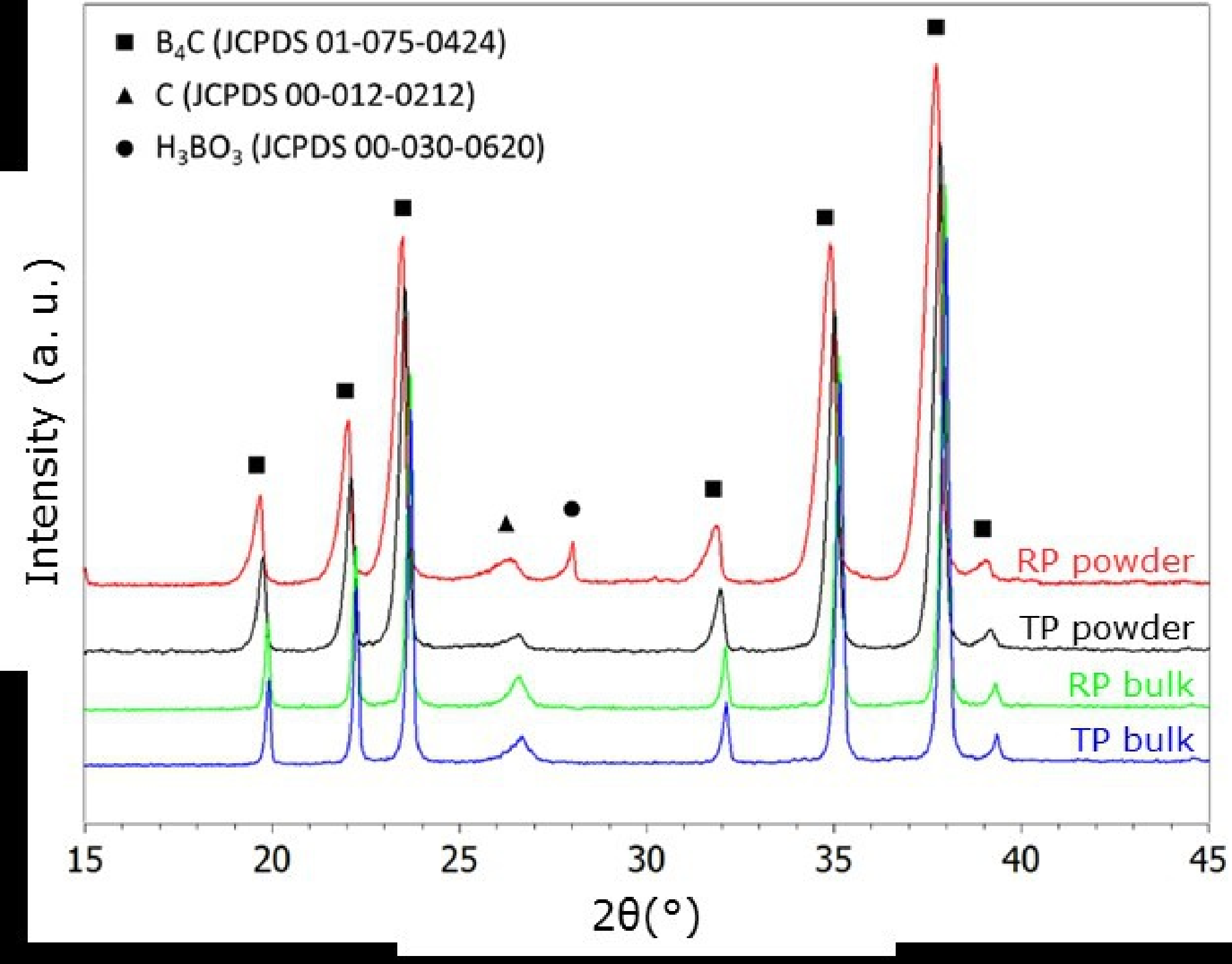
■ B_4C (JCPDS 01-075-0424)
▲ C (JCPDS 00-012-0212)
● H_3BO_3 (JCPDS 00-030-0620)
Intensity (a. u.)
RP powder
TP powder
RP bulk
TP bulk
15
20
25
30
35
40
45
2θ(°)

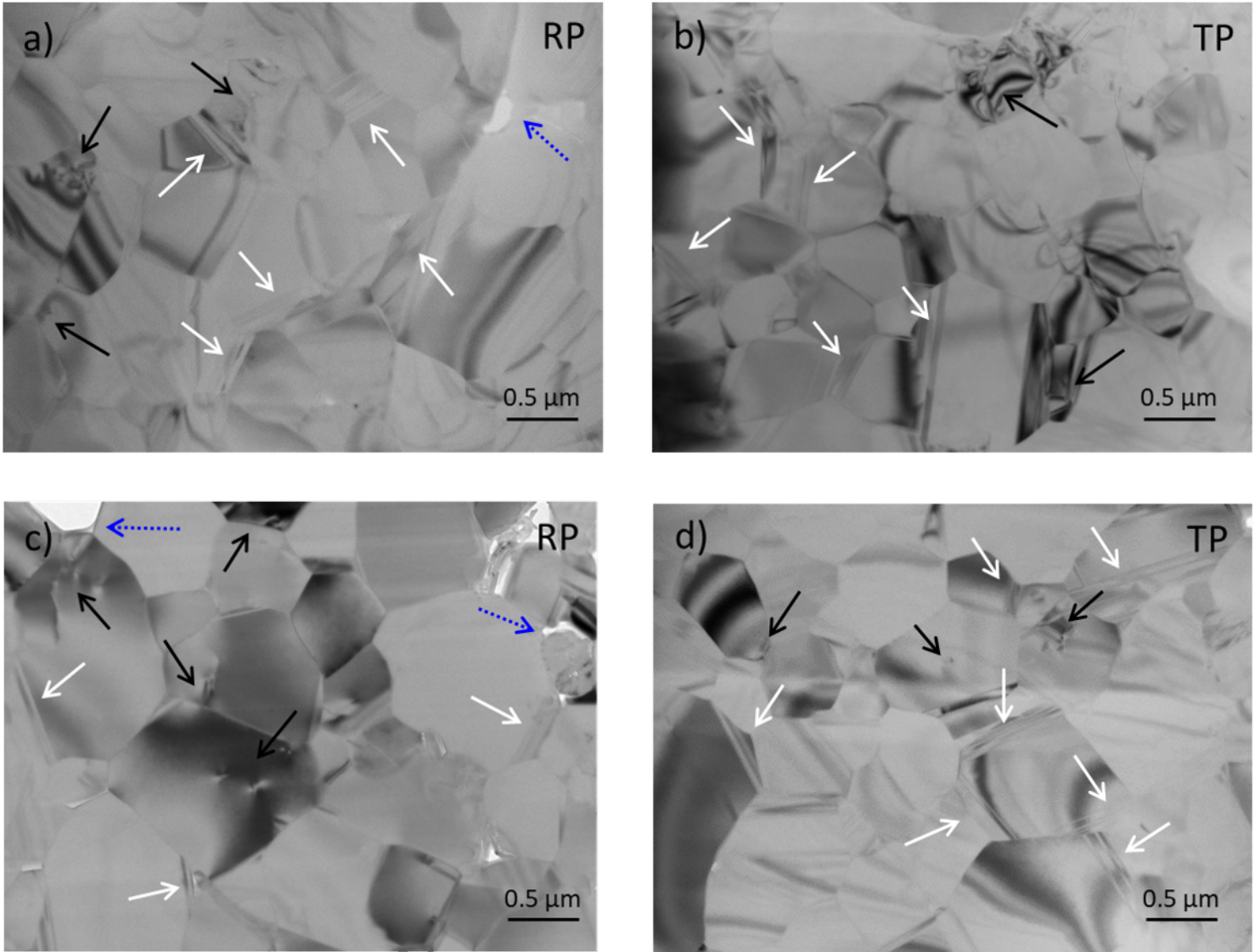
a)
RP
0.5 µm
b)
TP
0.5 µm
c)
RP
0.5 µm
d)
TP
0.5 µm

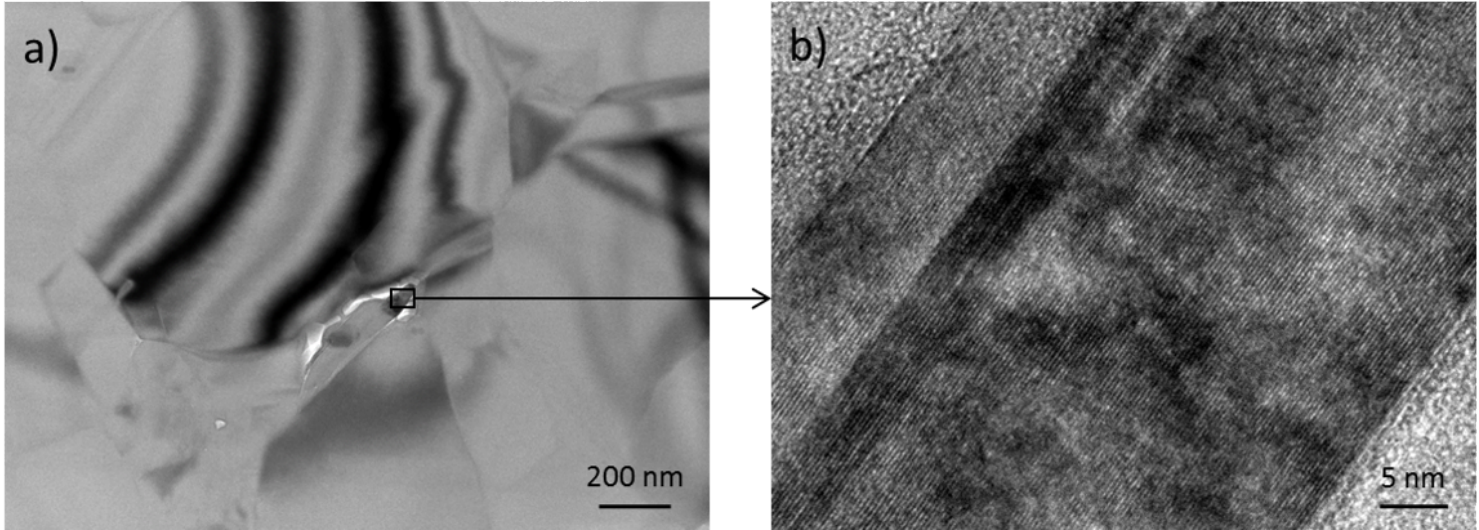
a)
200 nm
b)
5 nm

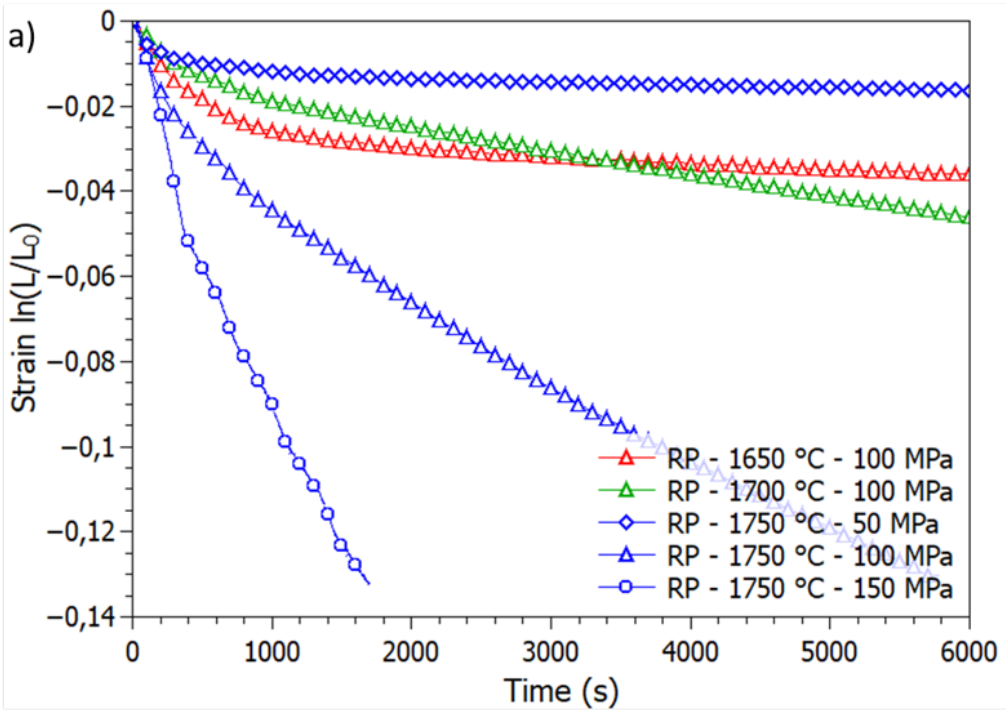
a)
Strain ln(L/L0)
0
−0,02
−0,04
−0,06
−0,08
−0,1
−0,12
−0,14
0
1000
2000
3000
4000
5000
6000
Time (s)
RP - 1650 °C - 100 MPa
RP - 1700 °C - 100 MPa
RP - 1750 °C - 50 MPa
RP - 1750 °C - 100 MPa
RP - 1750 °C - 150 MPa

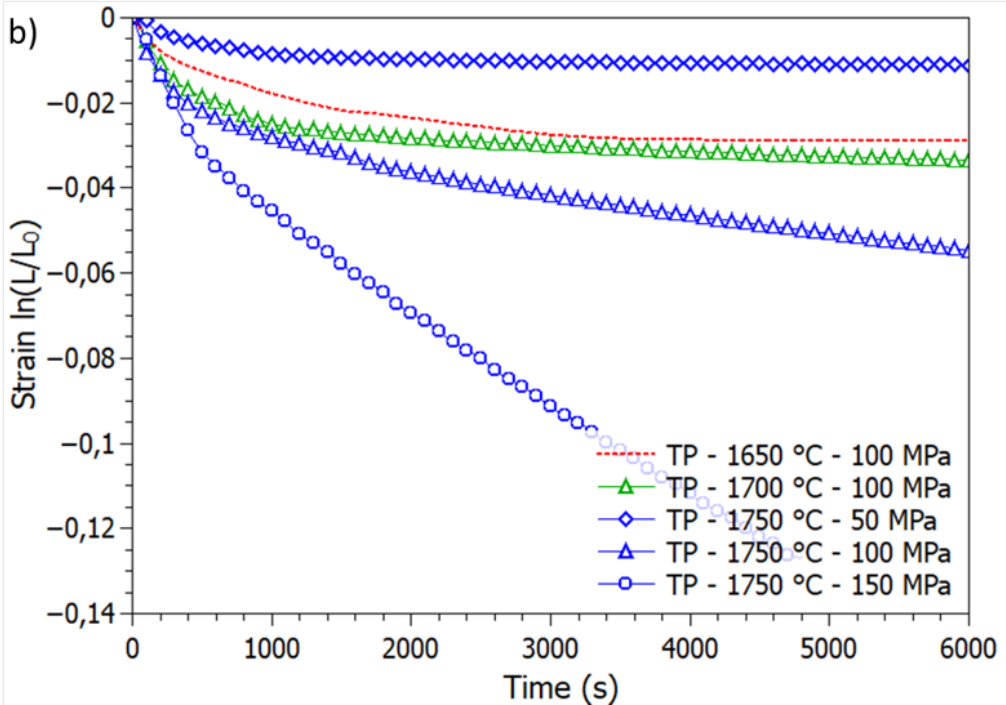
b)
Strain ln(L/L0)
0
−0,02
−0,04
−0,06
−0,08
−0,1
−0,12
−0,14
0
1000
2000
3000
4000
5000
6000
Time (s)
TP - 1650 °C - 100 MPa
TP - 1700 °C - 100 MPa
TP - 1750 °C - 50 MPa
TP - 1750 °C - 100 MPa
TP - 1750 °C - 150 MPa

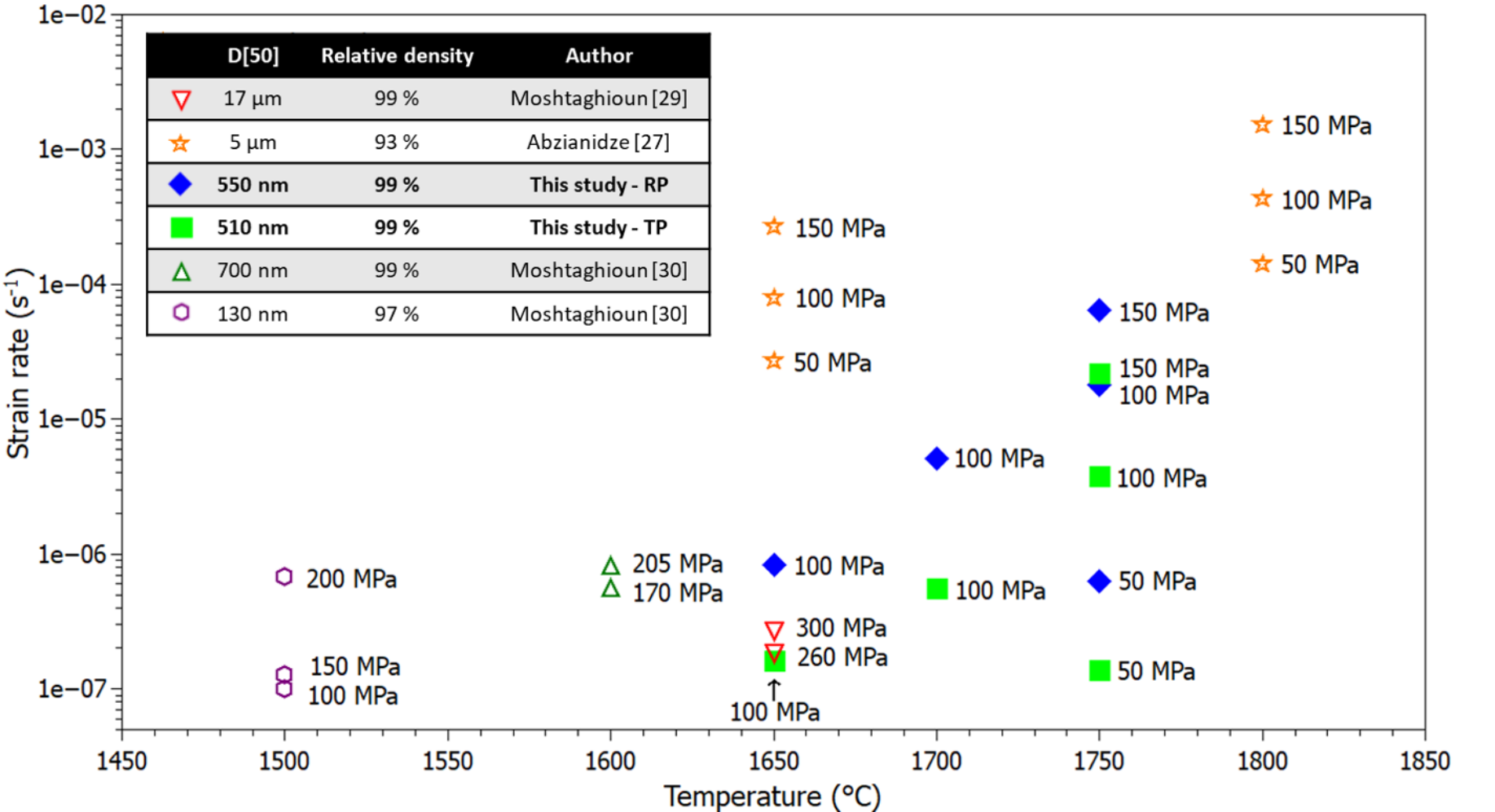
D[50] | Relative density | Author
17 µm | 99 % | Moshtaghioun [29]
5 µm | 93 % | Abzianidze [27]
550 nm | 99 % | This study - RP
510 nm | 99 % | This study - TP
700 nm | 99 % | Moshtaghioun [30]
130 nm | 97 % | Moshtaghioun [30]
Strain rate (s-1)
1e−02
1e−03
1e−04
1e−05
1e−06
1e−07
Temperature (°C)
1450
1500
1550
1600
1650
1700
1750
1800
1850
150 MPa
100 MPa
50 MPa
150 MPa
100 MPa
50 MPa
150 MPa
100 MPa
100 MPa
100 MPa
200 MPa
205 MPa
170 MPa
100 MPa
100 MPa
50 MPa
300 MPa
260 MPa
50 MPa
150 MPa
100 MPa
100 MPa

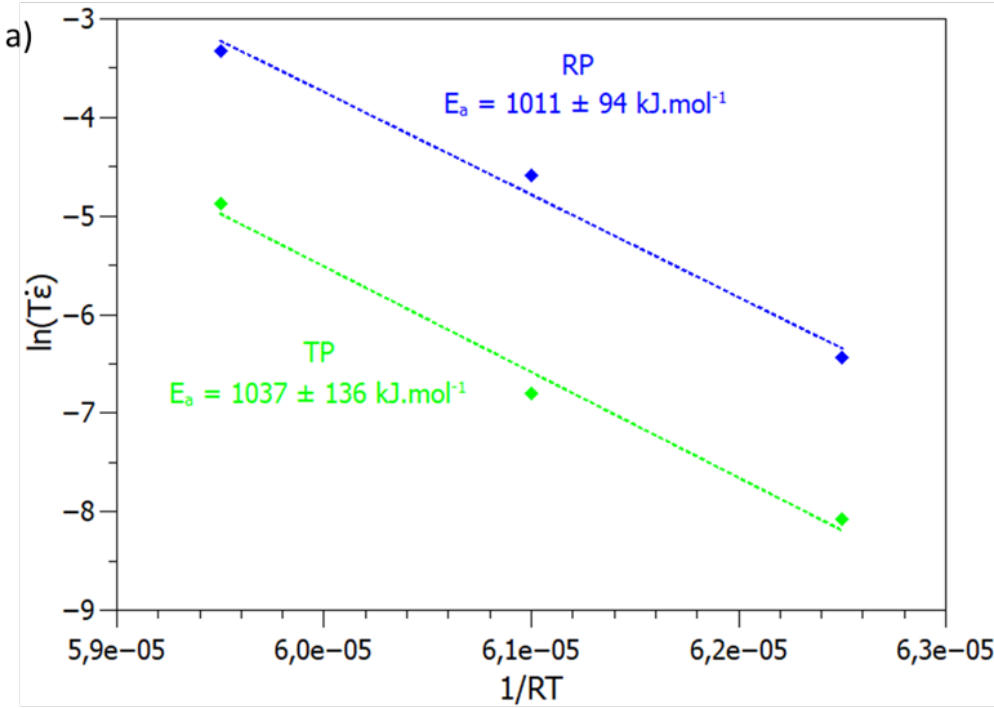
a)
RP
E_a = 1011 ± 94 kJ.mol^{-1}
TP
E_a = 1037 ± 136 kJ.mol^{-1}
ln(Tε̇)
1/RT
−3
−4
−5
−6
−7
−8
−9
5,9e−05
6,0e−05
6,1e−05
6,2e−05
6,3e−05

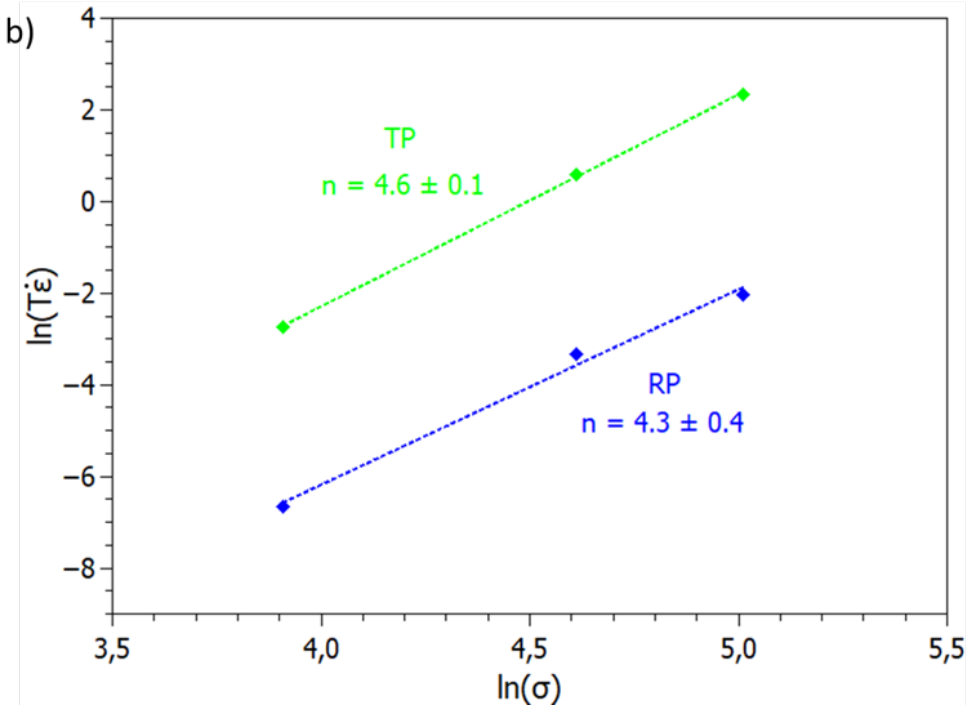
b)
TP
n = 4.6 ± 0.1
RP
n = 4.3 ± 0.4
ln(Tε̇)
ln(σ)
4
2
0
−2
−4
−6
−8
3,5
4,0
4,5
5,0
5,5

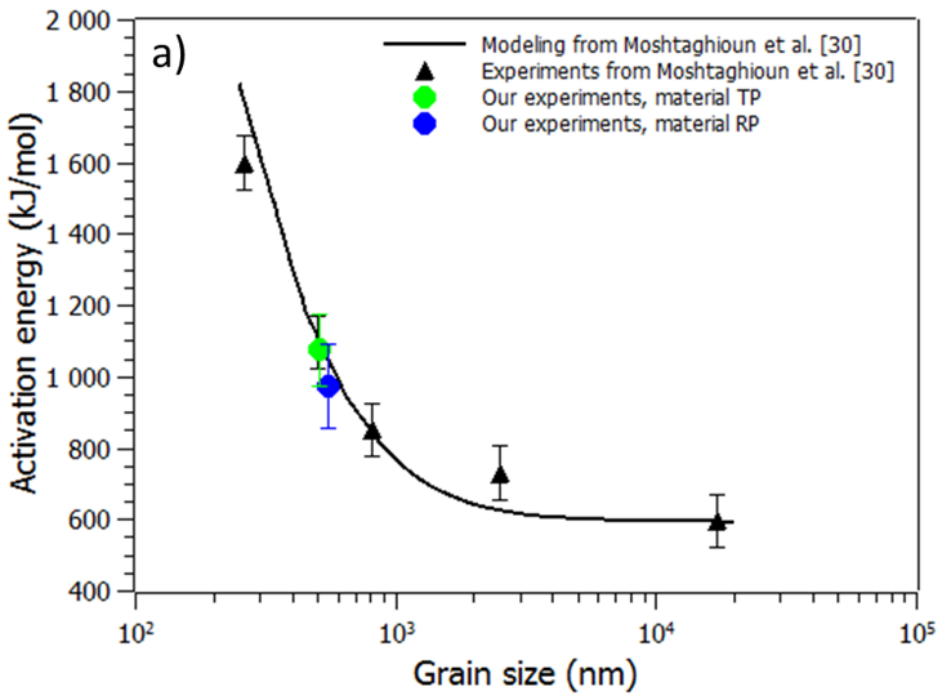
a)
Modeling from Moshtaghioun et al. [30]
Experiments from Moshtaghioun et al. [30]
Our experiments, material TP
Our experiments, material RP
Activation energy (kJ/mol)
2 000
1 800
1 600
1 400
1 200
1 000
800
600
400
10^2
10^3
10^4
10^5
Grain size (nm)

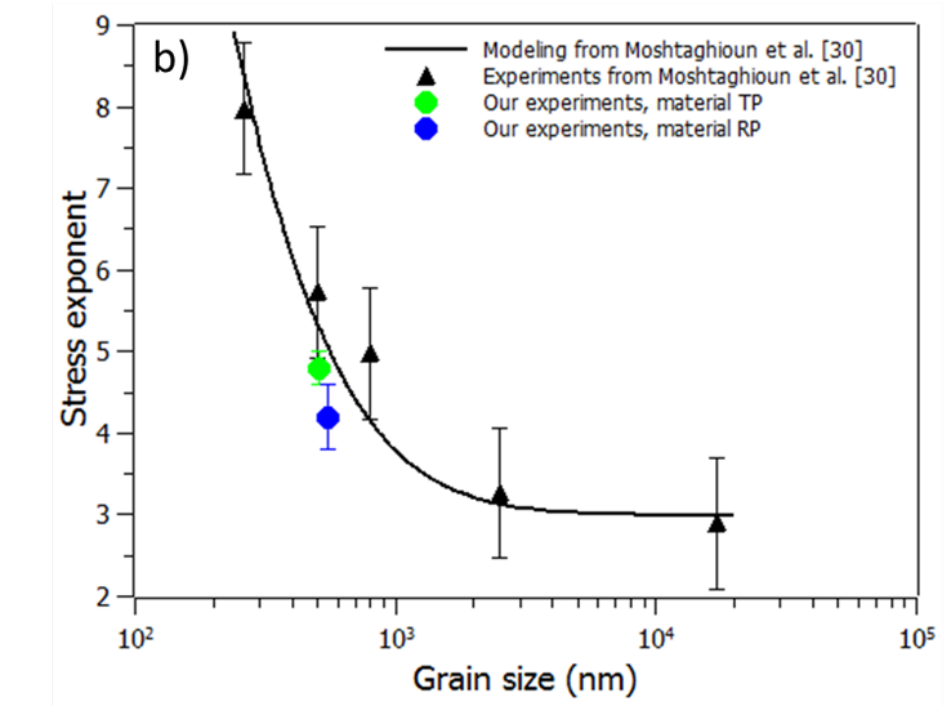
b)
Modeling from Moshtaghioun et al. [30]
Experiments from Moshtaghioun et al. [30]
Our experiments, material TP
Our experiments, material RP
Stress exponent
9
8
7
6
5
4
3
2
10^2
10^3
10^4
10^5
Grain size (nm)